

Final Draft
of the original manuscript:

Dami, S.; Abetz, C.; Fischer, B., Radjabian, M.; Georgopoulos, P.; Abetz, V.:
**A correlation between structural features of an amphiphilic
diblock copolymer in solution and the structure of the porous
surface in an integral asymmetric membrane**
In: Polymer (2017) Elsevier

DOI: 10.1016/j.polymer.2017.05.024

A Correlation between Structural Features of an Amphiphilic Diblock Copolymer in Solution and the Structure of the Porous Surface in an Integral Asymmetric Membrane

Sofia Dami¹, Clarissa Abetz¹, Birgit Fischer², Maryam Radjabian¹, Prokopios Georgopoulos¹, Volker Abetz^{1,2*}

¹Helmholtz-Zentrum Geesthacht, Institute of Polymer Research, Max-Planck-Straße 1, 21502 Geesthacht, Germany

²University of Hamburg, Institute of Physical Chemistry, Martin-Luther-King-Platz 6, 20146 Hamburg, Germany

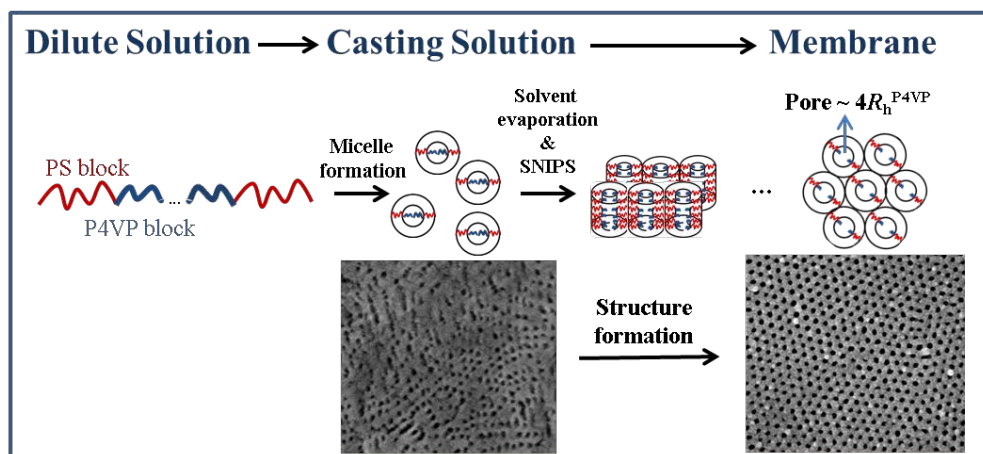
Abstract

A correlation between the pore size of isoporous block copolymer membranes produced *via* the combination of self-assembly with non-solvent induced phase separation (SNIPS) on one side and the macromolecular dimensions of the block copolymer in the casting solution on the other side is presented. Dilute solutions of a polystyrene-*b*-poly(4-vinylpyridine) (PS-*b*-P4VP) diblock copolymer and corresponding polystyrene (PS) and poly(4-vinylpyridine) (P4VP) homopolymers similar to the respective blocks of the diblock copolymer are investigated separately by static and dynamic light scattering (SLS, DLS) in solvent mixtures of tetrahydrofuran/ *N,N*-dimethylformamide (THF/DMF). These measurements provide information about the size of the individual polymers in solution. Solutions of the diblock copolymer at higher concentrations are studied furthermore by small-angle X-ray scattering (SAXS) and cryogenic scanning electron microscopy (cryo-SEM) in order to estimate the size of self-assembled structures in concentrated solution, as well as by scanning electron microscopy (SEM) in the final membrane. The pore radius of the selective layer in the resulting membrane obtained by SNIPS is shown to be similar to the hydrodynamic diameter of the pore forming block, as determined in dilute solution.

Keywords:

Keywords: Diblock copolymer in solution, Isoporous membrane, Self-assembly, Hydrodynamic radius, Radius of gyration, Membrane pore size

Graphical Abstract



1 Introduction

Block copolymers have gained an immense interest over the last decades. Their ability to self-assemble and microphase separate leads to several structures such as spheres, cylinders, double gyroids, lamellae or more complex structures with regard to the number of blocks, the architecture or the use of additives. [1-15] A large amount of information has been revealed after many studies on their behavior in bulk [16-18] or in solution in an appropriate solvent or solvent mixture. [19-33] Additionally, block copolymers received interest as bulk materials, but also as compatibilizers, blends or templates for nanopatterning. [34-38] Lately, they are also used for developing different types of membranes, such as dense membranes for gas separation from multiblock copolymers [39, 40] or porous membranes mostly from diblock copolymers for ultrafiltration. [41-50]

In this work, we study solutions of polystyrene-*b*-poly(4-vinylpyridine) (PS-*b*-P4VP) used for fabrication of isoporous integral asymmetric block copolymer membranes via self-assembly and non-solvent induced phase separation (SNIPS) and compare structural features of the block copolymer in solution with the finally formed membrane. [42] The isoporous membranes are formed by casting a solution using a doctor blade, where the block copolymer is dissolved in a proper solvent or solvent mixture, onto a flat substrate. Then a part of the solvent evaporates what induces the build-up of a gradient of the solvent concentration from the upper surface towards the bottom, initiating microphase separation and directing it along the gradient before the following immersion into a non-solvent precipitation bath traps the formed structure. This procedure was first developed for casting flat sheet membranes by doctor blading but has also been successfully transferred to the fabrication of hollow fiber membranes [51-54] or spraying membranes [55]. There are several parameters affecting the structure occurring in solution and in the final membrane, with the most important ones being the incompatibility between the different polymer blocks, the block copolymer composition, and the solvent selectivity. The solvent quality for each block affects the critical micelle concentration and may lead to different structures. [30, 56, 57] Several additives which selectively interact with the pore forming block have been used in order to enhance the formation of an isoporous surface layer, and it was shown that different additives might result in different pore sizes. [58-60]

Different methods have been used to investigate the structure formation in membrane casting solutions. Small-angle X-ray scattering (SAXS) can give information on the structure in solution. [61, 62] Structure evolution during evaporation of solvent has also been followed by the *in situ* SAXS. [32] The influence of the addition of small amounts of non-solvent to a block copolymer solution was investigated by small angle neutron scattering (SANS).[30] Another powerful method to investigate structures in solutions at high concentrations is cryo-scanning electron microscopy (cryo-SEM). Oss-Ronen et. al. [30] studied the micellar and structural evolution in solutions in this way while later Marques et. al. studied the block copolymer membrane formation through time-resolved GISAXS and cryo-microscopy characterization. [31]

The objective of the present work is to find a relationship between structural features of a diblock copolymer in solution and the surface structure of the final membrane obtained by the SNIPS process. The system under investigation consists of polystyrene (PS), poly(4-vinylpyridine) (P4VP) homopolymers and PS-*b*-P4VP diblock copolymer in tetrahydrofuran (THF) / *N,N*-dimethylformamide (DMF) solvent mixtures with, the first solvent being selective for the PS block and the second being slightly selective for the P4VP block. In order to have a better understanding of the behavior of the diblock copolymer in the dilute region, the hydrodynamic radius, R_h , of PS-*b*-P4VP is investigated in different solvents and solvent mixtures. Since a combination of THF and DMF has been widely used for the preparation of isoporous integral asymmetric membranes from this type of diblock copolymer, [42, 63] we focus our work accordingly, with the aim to observe the structure and pore formation process. The basic criterion for the selection of this system is that the solvent mixture can dissolve both blocks, giving the opportunity to observe better each step. This includes the observation of the starting random coil, the micelle formation as well as the structure formed in the final membrane with increasing concentration in a changing solvent due to the selective evaporation of THF.

2 Experimental Part

2.1 Materials

The PS and P4VP homopolymers, as well as the PS-*b*-P4VP diblock copolymer, were synthesized *via* anionic polymerization. [63] For the synthesis of PS homopolymer and PS-*b*-

P4VP diblock copolymer (THF) was used as a solvent. It was purified by successive distillation from molecular sieves and *sec*-butyllithium. Styrene was cleaned *via* aluminum oxide column and distillation over dibutylmagnesium. 4-Vinyl pyridine was purified via distillation from calcium hydride and ethylaluminium dichloride. The polymerization was carried out at -78 °C. The polymerization of styrene was initiated with *sec*-butyllithium. In the case of the synthesis of the homopolymer at that point, the polymerization was terminated with a mixture of degassed methanol/ acetic acid. In the case of the diblock copolymer after a small aliquot extraction for characterization, the 4-vinyl pyridine monomer was added in the solution and left to polymerize overnight at -78 °C. The polymerization was terminated with a mixture of degassed methanol/ acetic acid. The polymers were precipitated in water and dried under vacuum. The composition of the diblock copolymer was determined by ¹H-NMR spectroscopy. For the polymerization of P4VP the solvent was anhydrous pyridine, and the initiation was done with the use of *sec*-butyllithium at -20 °C. The solution was left overnight under stirring at -20 °C and the termination was done with degassed methanol/ acetic acid mixture. Ethyl acetate was used as precipitant. The sample was thoroughly dried under vacuum. Molecular weights and polydispersity indexes of the PS precursor and PS-*b*-P4VP diblock copolymer, as well as P4VP homopolymer, were determined by gel permeation chromatography (GPC), at 50 °C, with dimethylacetamide as a solvent. The GPC was calibrated with polystyrene standards.

For the structural investigations of the polymer solutions THF and DMF (99.8%, Merck, Germany) were used without any further purification. For the polymers the following nomenclature is used: in PS^c, P4VP^c and PS_a-*b*-P4VP_b^c, a and b are the PS and P4VP weight fractions in the diblock copolymer, while c is the total weight average molecular weight (M_w) of the homopolymers and the diblock copolymer in kg/mol. All concentrations and solvent ratios are given in wt% unless specified otherwise.

2.2 Membrane Formation

The membrane was prepared *via* the SNIPS process as described elsewhere. [42] A PS_{80.2}-*b*-P4VP_{19.8}¹⁴⁶ diblock copolymer solution of a 26.5 wt% concentration in a solvent mixture of

THF/DMF: 35/65 was prepared and stirred for 48h. After stirring, it was cast onto a glass substrate to form the flat sheet membrane and to easily detach it for further SEM investigations. The casting procedure was done manually using a doctor blade at a height of 200 μm and the cast film was left for 2 sec under room atmosphere before immersion in Millipore water (0.055 $\mu\text{S}/\text{cm}$) where it was left overnight for completion of the solvent-non-solvent exchange. Before the investigation, it was dried at 60 $^{\circ}\text{C}$ for 48 h under vacuum.

2.3 Characterization Methods

2.3.1 Dynamic Light Scattering

Dynamic light scattering (DLS) measurements were conducted on an ALV/CGS-3 Compact Goniometer using an ALV/LSE-5003 Multiple Tau Digital Correlator equipped with a Nd:YAG Laser emitting at a wavelength of $\lambda=532$ nm. The measurements were done at different scattering angles (40-140 $^{\circ}$) and the temperature was kept constant at 25 $^{\circ}\text{C}$. Solutions with a concentration of 0.1 g/L were prepared for the PS and PS-*b*-P4VP polymers and of 0.5 g/L for P4VP homopolymer in different solvents and solvent mixtures.

2.3.2 Static Light Scattering

The static light scattering (SLS) measurements were conducted on an ALV/CGS-3 Compact Goniometer equipped with a He/Ne Laser using an ALV/LSE-5003 Multiple Tau Digital Correlator emitting at a wavelength of $\lambda = 632.8$ nm. The temperature was kept constant at 25 $^{\circ}\text{C}$. Several solutions with concentrations varying from 0.1-1.5 g/L were prepared. The solvent mixture used in these measurements was THF/DMF in a ratio of 40/60 and 10/90.

All solutions used for static and dynamic light scattering experiments were left to dissolve in the solvent mixture for 24 h and filtered through 0.45 μm polytetrafluoroethylene (PTFE) filters prior to use.

2.3.3 Small-Angle X-Ray Scattering

Small-angle X-ray (SAXS) scattering experiments were performed at the Beamline P12 of Petra III synchrotron storage ring at DESY in Hamburg, Germany. A Pilatus 2M detector was used at a

distance of 3.0 m. The exposure time was 0.05 s and the exposure period 1 s. A total number of 20 frames were acquired per measurement. The beam size was 0.1 x 0.2 mm² and the energy 10 keV. For the SAXS experiments, a small amount of the polymer solution was inserted in special glass capillaries. The scattering intensity I was analyzed as a function of the scattering vector q . The solution concentrations were in a range from 10 to 33wt% in different solvent mixtures.

2.3.4 Cryo-Scanning Electron Microscopy

Cryo-Scanning Electron Microscopy (cryo-SEM) experiments were performed on a LEO-Gemini 1550VP (Carl Zeiss, Germany) scanning electron microscope. In order to achieve the cryo-SEM images of the polymer solutions, a special sample preparation was necessary. A droplet of the solution was placed between two gold coated platelets and plunged in liquid ethane for a few seconds. Then, it was rapidly immersed in liquid nitrogen, LN₂ and inserted into a suitable specimen holder for mirror fracturing that was already frozen. Following that, the sample was transferred into the sputtering machine chamber of the BAL-TEC MED 020, held at -140 °C with the use of the Leica EM VCT100 vacuum cryo-transfer system. Inside the chamber, the solution droplet was freeze fractured by rapidly opening the two gold platelets, and the procedure was followed by slight sublimation at -100 °C for 1 min in the case of the more concentrated solutions and up to 3 min for the more diluted, in order to avoid any ice contamination. At this step, the sample is also coated with platinum as a conductive layer. After this, the sample was transferred to the microscope equipped with a cryo-stage, held at -130 °C for imaging by using a secondary electron (SE2) detector at an accelerating voltage of 1-2 kV and a working distance of approximately 6 mm. The images were taken of the surfaces of the broken sample, as close as possible to the center of the droplet in order to avoid any area from the outer surface where part of the solvent might have evaporated. The concentrations of the solutions under investigation were at a range of 25 to 33wt% in different solvent mixtures.

2.3.5 Scanning Electron Microscopy

Scanning electron microscopy (SEM) experiments on membranes were also done on the Leo-Gemini 1550VP. For the investigation of the surface, part of the membrane was placed in a

sample holder and coated with ca. 2 nm of platinum as a conductive layer. A secondary electron In-Lens detector was used for imaging at an accelerating voltage of 5 kV. The average pore diameters were determined by using the Analysis software (Olympus, Germany).

3 Results and Discussion

As already mentioned before, the aim of this work is to present a method for prediction of the pore size in the final structure of block copolymer membranes obtained by the SNIPS process by investigating the structure of the block copolymer in the casting solution. We investigated solutions of a PS_{80.2}-*b*-P4VP_{19.8}¹⁴⁶ diblock copolymer and the corresponding PS¹²⁰ and P4VP³⁷ homopolymers in mixtures of THF and DMF. The characteristics of the used polymers are given in Table 1.

Table 1: Molecular weight (M_w), polydispersity index (PDI) and weight fraction of each block (PS, P4VP) in the respective polymer.

	M_w (kg mol ⁻¹)	PDI	PS (wt%)	P4VP (wt%)
PS ¹²⁰	120	1.04	100	-
P4VP ³⁷	37	1.57	-	100
PS _{80.2} - <i>b</i> -P4VP _{19.8} ¹⁴⁶	146	1.06	80.2	19.8

The Hansen solubility parameters of each polymer and solvent indicate a selectivity of THF to PS and of DMF to P4VP, respectively, as shown in Table 2. The concentrations of diblock copolymer in the casting solutions in THF/DMF solvent mixtures are typically high (in the range of approx. 20-34 wt%). [63] Substitution by a more selective solvent such as 1,4-dioxane can change the concentration of the casting solution. [31, 55, 61, 62]

Table 2: Dispersion, polarity, hydrogen bonding, and total solubility parameters of the polymers and the solvents. [64-66]

	δ_D [MPa] ^{1/2}	δ_P [MPa] ^{1/2}	δ_H [MPa] ^{1/2}	δ_{total} [MPa] ^{1/2}
Polymers				
PS	18.5	4.5	2.9	19.3
P4VP	19.3	8.2	0.0	21.0
Solvents				
THF	16.8	5.7	8	19.4
DMF	17.4	13.7	11.3	24.9
1,4-Dioxane	19.0	1.8	7.4	20.4

Based on the solubility parameters, the Flory-Huggins interaction parameter, χ , can be estimated between the polymers, or the polymer and the solvent according to equation (1):

$$\chi_{12} = \frac{V}{RT} [(\delta_{D1} - \delta_{D2})^2 + 0.25(\delta_{P1} - \delta_{P2})^2 + 0.25(\delta_{H1} - \delta_{H2})^2] \quad (1)$$

χ_{12} : Flory-Huggins interaction parameter; V : molar volume of polymer segment or solvent; R : gas constant; T : temperature in Kelvin; $(\delta_{D1} - \delta_{D2})$, $(\delta_{P1} - \delta_{P2})$ and $(\delta_{H1} - \delta_{H2})$: the difference between dispersion, polarity and hydrogen bonding solubility parameters, respectively

The χ parameter estimated for the PS and P4VP homopolymers from the solubility parameters at a temperature of 25 °C is 0.25, but higher values are also reported from literature ($\chi > 1$ or $0.30 < \chi \leq 0.35$). [26, 67] Therefore the large value indicates a strong segregation tendency between the two polymers. For the PS_{80.2}-*b*-P4VP_{19.8}¹⁴⁶ used in this work, a $\chi N=350$ value is estimated, which is much higher than 10 [68], indicating that the two blocks are strongly segregated (N : degree of polymerization).

3.1 Investigation of Dilute Solutions

For our work, it was important to use a good solvent mixture in order to dissolve both polymer blocks at very low concentrations (~0.1 wt%), so that we can determine the length scale of the block copolymer and relate it to the length scale of the aggregates in more concentrated solutions or in the final membrane (especially the pore diameter). As the diblock copolymer is composed of two blocks, we also investigated the PS¹²⁰ and P4VP³⁷ homopolymers with approximately comparable molecular weight to the corresponding blocks of the diblock copolymer separately. Additionally, we compared their size with the one of each microphase separated component in the concentrated solutions and in the final membrane.

Firstly, several measurements were done by DLS in order to determine the size (hydrodynamic radius, R_h) of each homopolymer and the diblock copolymer in dilute solution.

In all cases, the R_h , was calculated via the translational diffusion coefficient, which was obtained from the intensity autocorrelation function (2):

$$g_2(q, t) = \frac{\langle I(q, t)I(q, t+\tau) \rangle}{\langle I(q, t)^2 \rangle} \quad (2)$$

$g_2(q, t)$: intensity autocorrelation function, q : wave vector, t : time, τ : correlation time

A second order cumulant fit (3) gives a mean decay rate $\bar{\Gamma}$:

$$\ln[g_2(q, t) - 1] = \ln\left(\frac{\beta}{2}\right) - \bar{\Gamma}t + \frac{\kappa_2}{2}t^2 \quad (3)$$

β : correction factor, $\bar{\Gamma}$: mean decay rate, κ_2 : second order cumulant

The translational diffusion coefficient, D_s , was calculated from the decay rate, $\bar{\Gamma}$ (4):

$$D_s = \frac{\bar{\Gamma}}{q^2} \quad (4)$$

and the R_h according to the Stokes-Einstein equation (5):

$$D_s = \frac{kT}{6\pi\eta R_h} \quad (5)$$

k : Boltzmann constant, T : temperature, η : solvent viscosity

The R_h of the polymers are given in Table 3 below. Additionally, in Figures **S1** and **S2** in supplementary information, the Γ is presented as a function of the q^2 of PS¹²⁰, P4VP³⁷ and PS_{80.2-}

b -P4VP_{19.8}¹⁴⁶ polymers in two solvent mixtures of THF/DMF: 20/80 and 50/50, respectively. The slope of the **linear** plots gives the diffusion coefficient D_s that leads to the R_h .

Table 3: Average hydrodynamic radius (R_h) of the homopolymers and the diblock copolymer measured by dynamic light scattering in dilute solutions

Ratio THF/DMF (wt%/wt%)	R_h (P4VP ³⁷) (nm) (0.5 g/L)	R_h (PS ¹²⁰) (nm) (0.1 g/L)	R_h (PS _{80.2} - b -P4VP _{19.8} ¹⁴⁶) (nm) (0.1 g/L)
0/100	4.6	8.4	9.8
10/90	4.5	8.4	9.4
20/80	4.5	8.2	9.6
30/70	4.6	8.7	10.2
35/65	4.6	8.7	9.8
40/60	4.6	8.6	9.1
50/50	4.5	9.2	10.1

The radii of gyration, R_g , of the polymers were measured separately in a solvent mixture of THF/DMF: 40/60 by static light scattering in order to correlate them to the R_h measured by dynamic light scattering. The ρ ratio indicates the scattering particle topology and is defined as (6):

$$\rho_{\text{ratio}} = R_g / R_h \quad [69] \quad (6)$$

and in the literature is referred to be $\rho_{\text{ratio}} = 1.505$ for random polymer coils. [69]

Several dilute solutions were measured in order to determine the M_w the second virial coefficient, A_2 , and the R_g according to the Zimm equation (7):

$$\frac{Kc}{R_\theta} = \frac{1}{M_w} \left(1 + \frac{1}{3} R_g^2 q^2 \right) + 2A_2c \quad (7)$$

R_θ : Rayleigh ratio

c : solution concentration

K : contrast factor (8)

$$K = \frac{2\pi^2\eta^2}{\lambda^4 N_A} \left(\frac{dn}{dc}\right)^2 \quad (8)$$

λ : wavelength, N_A : Avogadro Number, η : viscosity of the solvent and dn/dc : refractive index increment.

q : scattering vector (9)

$$q = 4\pi n_0 \sin(\theta/2)/\lambda \quad (9)$$

n_0 : refractive index of the solvent

For these measurements, at first it was necessary to determine the refractive index increment, dn/dc , of each block of the diblock copolymer separately. Then, the refractive index increment of the block copolymer can be calculated from the individual contributions. [70] In our case, the dn/dc values of PS¹²⁰ and P4VP³⁷ in the same solvent mixture of THF/DMF: 40/60 were 0.181 and 0.177, respectively. This similarity between these two polymers has also been observed before. [22] In Figure S3 (a), (b) and (c) in the supplementary information, the Zimm-plots of the homopolymers and the diblock copolymer in THF/DMF: 40/60 are shown. The molecular weights, second virial coefficients and R_h obtained by the Zimm-plot in static light scattering and also the molecular weights obtained by GPC are presented in Table S1 in the supplementary information.

As can be seen from the SLS results, the M_w obtained from static light scattering, is very similar to the one measured by GPC in the case of PS¹²⁰ and PS_{80.2}-*b*-P4VP_{19.8}¹⁴⁶ diblock copolymer. A considerable difference is noticed to the M_w values of the P4VP³⁷ homopolymer, due to the fact that polystyrene standards were used for GPC calibration. Additionally, the P4VP³⁷ homopolymer that exhibited a polydispersity of 1.57 was compared to the commercial P4VP⁴² homopolymer (Polymer Source Inc., Quebec, Canada) that has a lower polydispersity of 1.24 and no strong effects of the polydispersity on the scattering were identified.

Theoretical values for the radius of gyration, R_g , under θ -solvent conditions can be easily calculated. The end-to-end distance, r , for a random coil in dilute solution it is related to R_g by (10) [71-73] :

$$R_g^2 = \frac{r^2}{6} \quad (10)$$

The end-to-end distance, r , is obtained from Kuhn's law (11):

$$r^2 = i * N * l^2 * C \quad (11)$$

i : number of bonds per monomer unit, N : degree of polymerization, l : segmental length (length of a backbone bond), C : polymer characteristic ratio [62, 72, 73]

For the PS_{80.2}-*b*-P4VP_{19.8}¹⁴⁶ diblock copolymer, the degree of polymerization is $N_{PS} = 1125$, $N_{P4VP} = 275$. The segmental length is $l_{PS/P4VP} = 0.154$ nm, the characteristic ratio is $C_{PS} = 9.85$ and $i_{PS/P4VP} = 2$. The same characteristic ratio value was used also for P4VP. [72, 73]

Depending on the solvent quality, the proportionality of R_g to the N , is the following (12):

$$R_g \propto N^v \quad (12)$$

where v : 1/3, bad solvent; 1/2, θ solvent; 3/5 good solvent [71]

Concerning the polymers used in this work, in the case of PS¹²⁰, P4VP³⁷ and PS_{80.2}-*b*-P4VP_{19.8}¹⁴⁶ the expected R_g under θ -conditions would be ca. 10 nm, 5 nm, and 11 nm, respectively, considering the block copolymer behavior as the one of a homopolymer. Therefore, from the equation (12), in a good solvent, the radii would be approximately 20 nm, 8.5 nm, and 23 nm, respectively. Comparing the calculations for θ -solvent conditions to our experimental results indicates that the selected solvent mixture behaves as a good solvent for the polymers, showing a better quality in the case of P4VP³⁷, where the measured R_g is very close to the theoretical expected which is 8.5 nm. The above mentioned is also supported from the second virial coefficients reported in Table S1, where the value for the P4VP³⁷ is higher compared to the ones for PS¹²⁰ and PS_{80.2}-*b*-P4VP_{19.8}¹⁴⁶.

The R_g , is larger than the R_h for a random polymer coil. From the values in Tables 3 and S1, R_g exceeds the R_h by a factor of 2 for the P4VP³⁷ homopolymer, and by a factor of 1.7 and 1.6 for the PS¹²⁰ and PS_{80.2}-*b*-P4VP_{19.8}¹⁴⁶, respectively.

Taking advantage of the proportionality between R_g and R_h , we expect similar R_g for the polymer coils dissolved in the other solvent mixtures of this study, since there is no significant difference in the R_h reported in Table 3. This is also indicated from the Zimm-Plot presented in Figure S3 (d) corresponding to the solutions containing PS¹²⁰ in a solvent mixture of THF/DMF: 10/90 where the results are quite similar to the ones at a ratio of 40/60 (Figure S3 (a)). The second virial coefficients show a good solvent quality for the solvent mixtures used and are proportionally consistent with the ones for PS in THF ($A_2 = 7 \cdot 10^{-7}$ mol*dm³/g²) [73], and for PS in DMF ($A_2 = 1.8 \cdot 10^{-7}$ mol*dm³/g²) [74]. This is a strong indication that the behavior of the PS in the THF/DMF solvent mixtures we have used is very similar. Since PS is the dominant block in

the diblock copolymer, we consider that no significant difference should be noted in the other solutions. To conclude, no micelle formation is detected under these conditions, and the solvent effectively screens the repulsive interactions of the two blocks. Indeed, insufficient screening of the repulsive interactions will occur at higher concentrations, or if the solvent selectivity changes. Both occur upon membrane casting when the more volatile THF evaporates much faster than DMF before the system is quenched in the SNIPS process.

3.2 Investigation of Concentrated Solutions

The investigation of the more concentrated solutions was initiated by SAXS and followed by cryo-SEM. The idea behind the SAXS investigation is to monitor the evolution of the structure formation firstly by increasing the concentration of the diblock copolymer in a selected solvent mixture maintaining certain characteristics, e.g., volatility, as mentioned previously. This is a necessary step to find a concentration close to the transition between disordered micelles and an ordered structure. However, during membrane formation after solution casting, some part of the volatile solvent will evaporate. Therefore, the next step is to use this reference concentration which is close to the ordering transition and slowly decrease the amount of the volatile solvent in order to approach the point where the ordering occurs.

In order to achieve this, three sets of solutions were prepared in order to see at which concentration and solvent composition ordering occurs:

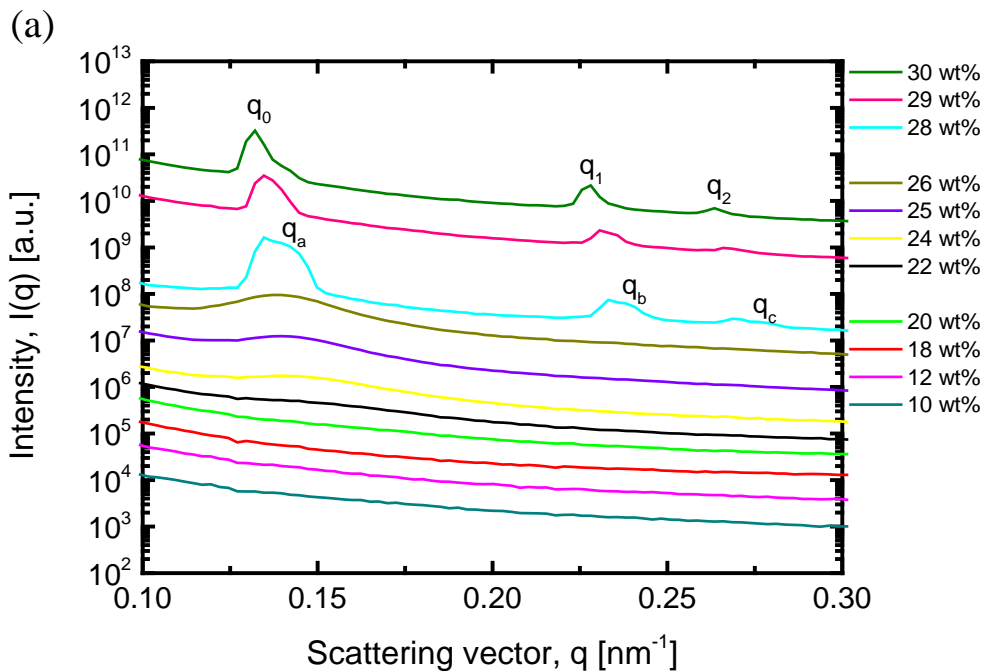
1. The first set of solutions consists of several concentrations at a range of 10-30 wt% $\text{PS}_{80.2}\text{-}b\text{-P4VP}_{19.8}$ ¹⁴⁶ in the same solvent mixture as in DLS and SLS, THF/DMF: 40/60.
2. The second set of solutions consists of several concentrations at a range of 26-29 wt% $\text{PS}_{80.2}\text{-}b\text{-P4VP}_{19.8}$ ¹⁴⁶ in the solvent mixture of THF/DMF: 30/70.
3. The third set consists of $\text{PS}_{80.2}\text{-}b\text{-P4VP}_{19.8}$ ¹⁴⁶ solutions in different solvent mixtures of THF/DMF, representing more closely the compositional changes in a membrane casting solution as a result of decreasing the THF amount in the solution during evaporation. Therefore the ratio between the polymer and DMF is kept the same.

The solution concentration was increased either by keeping the composition of solvent mixture constant or by decreasing the amount of THF while maintaining the proportion of polymer/DMF in the solutions constant. The results of the different SAXS experiments are presented in Figure 1.

The domain spacing d was calculated from the first peak using Bragg's law (13):

$$q^* = 2\pi/d \quad (13)$$

By the increase of the polymer concentration or change of the solvent ratio, besides the first peak, higher-order peaks appear in the SAXS curves. This indicates a transition from the disordered solution into a partially ordered or ordered structure. The peak sequence, q_i/q_0 , in all cases is 1: $\sqrt{3}$: $\sqrt{4}$, indicating a 2D hexagonally packed cylindrical structure starting at a concentration of 28 wt% in all cases. The domain spacing d was calculated in the range of approximately 46-47 nm. The analytical results are reported in Table S2.



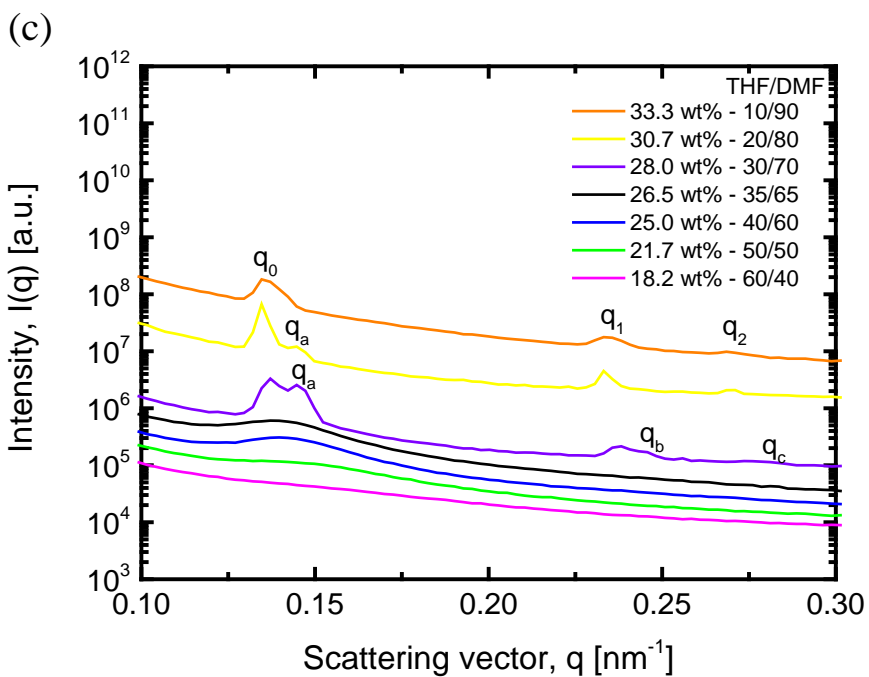
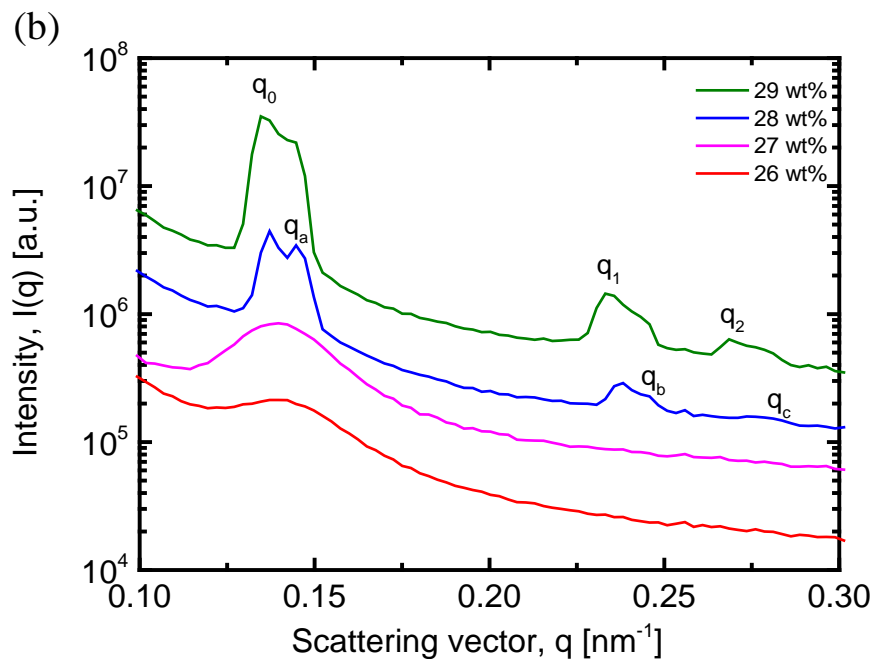


Figure 1: Scattering intensity I as a function of the scattering vector q from the SAXS experiments on the different polymer systems. More specifically, in (a) and (b) the influence of the concentration increase and in (c) the influence of the decrease of THF amount in the solutions are presented. The curves are vertically shifted for clarity.

The SAXS measurements showed that ordered structures can be formed in all three solution sets. In general, single broad peaks indicating disordered micelles in the solution can be clearly seen in all the presented curve sets in Figure 1 up to a solution concentration of 26-27 wt%. For all solutions with a concentration of 28 wt%, except from the first set of peaks (q_x , with $x = 0, 1, 2, 3\dots$), pronounced shoulders at higher q values (q_y , with $y = a, b, c\dots$) are visible. This indicates the presence of a second coexisting structure, with a domain spacing 3 - 4 nm smaller than the dominant structure. Decrease in their intensity with further increasing of the concentration leads to the conclusion that the transition from the disordered to the ordered solution structure occurs step by step. Taking this into account and also the quite high concentrations where ordered structure occurs, the broad peaks appearing from a 28 wt% polymer solution show a gradual structure build up. We investigated the increase of the concentration in steps of 1-2 wt% and found that ordering occurs at this specific concentration. However, this formed structure is either disturbed from micelles that are still not ordered or consist of a similar co-existing structure in the solution with slightly different domain spacing. In general, splitting peaks have been also observed in other recent works. [62, 75] In any case, by following the intensity of the shoulder in the broader peaks, these disordered micelles should be the minority, compared to the ordered ones. With the further increase of concentration the structure in the solution becomes homogeneous.

Cryo-SEM was used for further investigation of the solutions. The solutions correspond to the first set of the SAXS section above, where the polymer concentration was increased by diblock copolymer addition in the solution at a fixed THF/DMF ratio (Figure 1 (a)) and to the third one, where the concentration was increased by THF reduction in solutions with a fixed diblock copolymer/DMF ratio (Figure 1 (c)). [30, 62] The results of the cryo-SEM measurements corresponding the first SAXS solutions set are presented in the micrographs in Figure 2. In agreement with the SAXS results, the solutions show an increasing order of micelles for higher polymer concentrations. In the solution with 25 wt% concentration of diblock copolymer micelles are found, as shown in Figure 2 (a). It can be distinguished the minor P4VP blocks in the micelle core (darker parts) from the PS blocks forming the matrix (lighter parts) as has also been shown by Oss-Ronen et. al.. [30] With the increase of the concentration, more micelles will form, which tend to fuse into cylinders that will pack hexagonally in the solution. This can be clearly seen in Figure 2(b), corresponding to a solution concentration of 28 wt% of the diblock

copolymer. The same phenomenon is visible for the sample with 29 wt% diblock copolymer concentration (Figure 2(c) and (d)) and 30 wt% (Figure 2(e)).

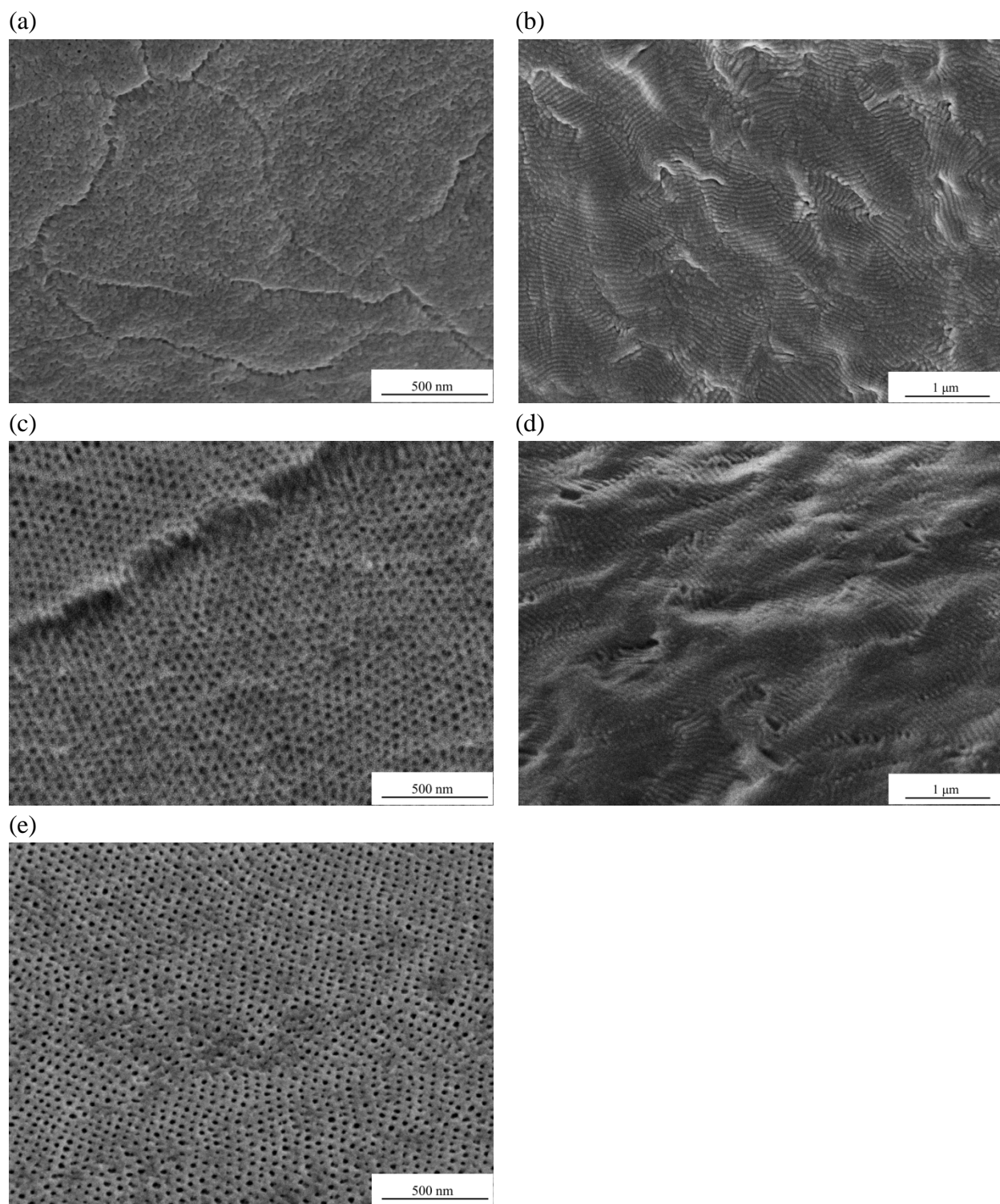


Figure 2: Cryo-SEM micrographs of $\text{PS}_{80.2}\text{-}b\text{-P4VP}_{19.8}^{146}$ diblock copolymer at different concentrations (a) 25 wt%; (b) 28 wt%; (c), (d) 29 wt% and (e) 30 wt% in the same solvent mixture THF/DMF: (40/60).

The second approach to systematically vary the solution composition corresponding to the third SAXS solutions set is presented in Figure 3. This strategy allows us to mirror the formation of a regular nanostructure on the top layer of the cast film, when a certain amount of the volatile solvent evaporated prior to immersion into water. The concentration of the solution increased due to solvent reduction. The first solution under investigation (Figure 3(a)) contained 25 wt% of diblock copolymer in THF/DMF: 40/60 and in the following, the THF amount was decreased in steps of 5 and 10 wt% until the solution composition became 33.3 wt% of diblock copolymer in THF/DMF: 10/90 (Figure 3(e)). The micelles come closer at a concentration of 26.5 wt% (Figure 3(b)) after reducing the THF amount at a range of 5 wt%, while after 10 wt% decrease they assembled in a well-ordered hexagonal structure (Figure 3(c)). By further reduction of THF and increase of the polymer concentration well-ordered cylinders were observed in the solution (Figure 3(d) and (e)).

To conclude, cryo-SEM investigations and SAXS showed the same micellar and structural evolution. Moreover, the distance between the cylinders in the cryo-SEM micrographs in both cases agrees with the domain spacing calculated from the SAXS measurements.

At this point should be noted that, as mentioned in the SAXS section, a second structure is visible in most cases in the cryo-SEM micrographs as well, where a sphere-like structure occurred mostly at a 28 wt% concentration in a THF/DMF: 40/60 and 30/70 solvent mixture in both sets of solutions. A transition from spheres to cylinders happens by further increase of the concentration, leading to a more regular 2D hexagonally packed cylindrical structure.

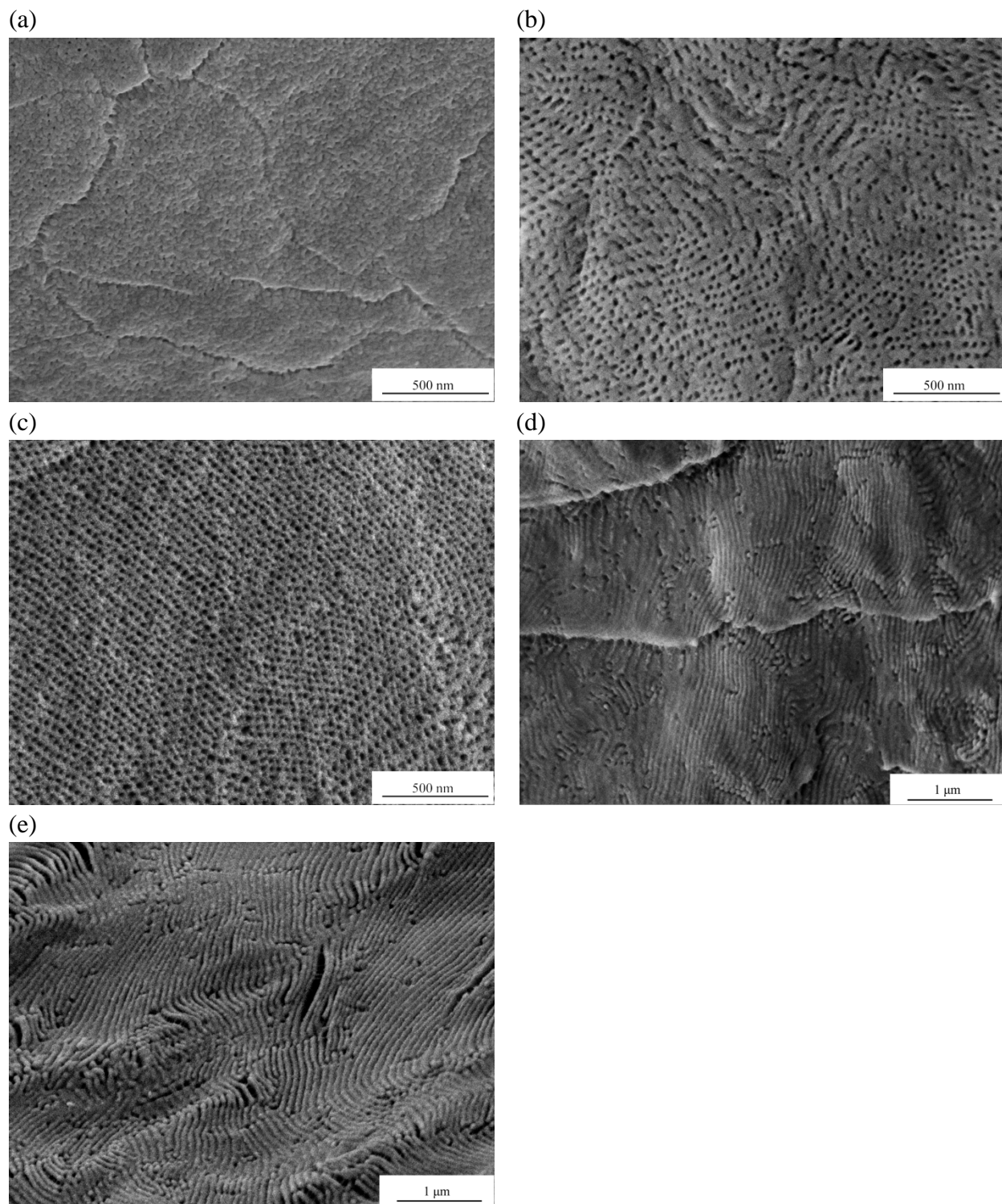


Figure 3: Cryo-SEM micrographs of $PS_{80.2}\text{-}b\text{-}P4VP_{19.8}$ block copolymer in different solvent mixture compositions (a) 25 wt% in THF/DMF: 40/60, (b) 26.5 wt% in THF/DMF: 35/65, (c) 28 wt% in THF/DMF: 30/70, (d) 30.7 wt% in THF/DMF: 20/80 and (e) 33.3 wt% in THF/DMF: 10/90.

3.3 Membrane Formation

Finally, we compare the structural information we gained from the solution studies with the surface layer of the integral asymmetric membrane. The solution of 26.5 wt% PS_{80.2}-*b*-P4VP_{19.8}¹⁴⁶ diblock copolymer, in THF/DMF: 35/65 was chosen as the casting solution since the SAXS results and cryo-SEM observations confirm that the solution concentration is very close to disorder-order transition. For this solution, we assumed that after a very short evaporation time (ca. 2 sec), the required amount of THF (at least 5wt%) will evaporate. Therefore the already close but still disordered micelles will fuse to the 2D hexagonal cylindrical structure as indicated by the above investigations. In Figure 4(a) a cryo-SEM image of the casting solution is shown, while in Figures 4(b) and (c) micrographs of the final dried membrane surface and cross section are presented accordingly.

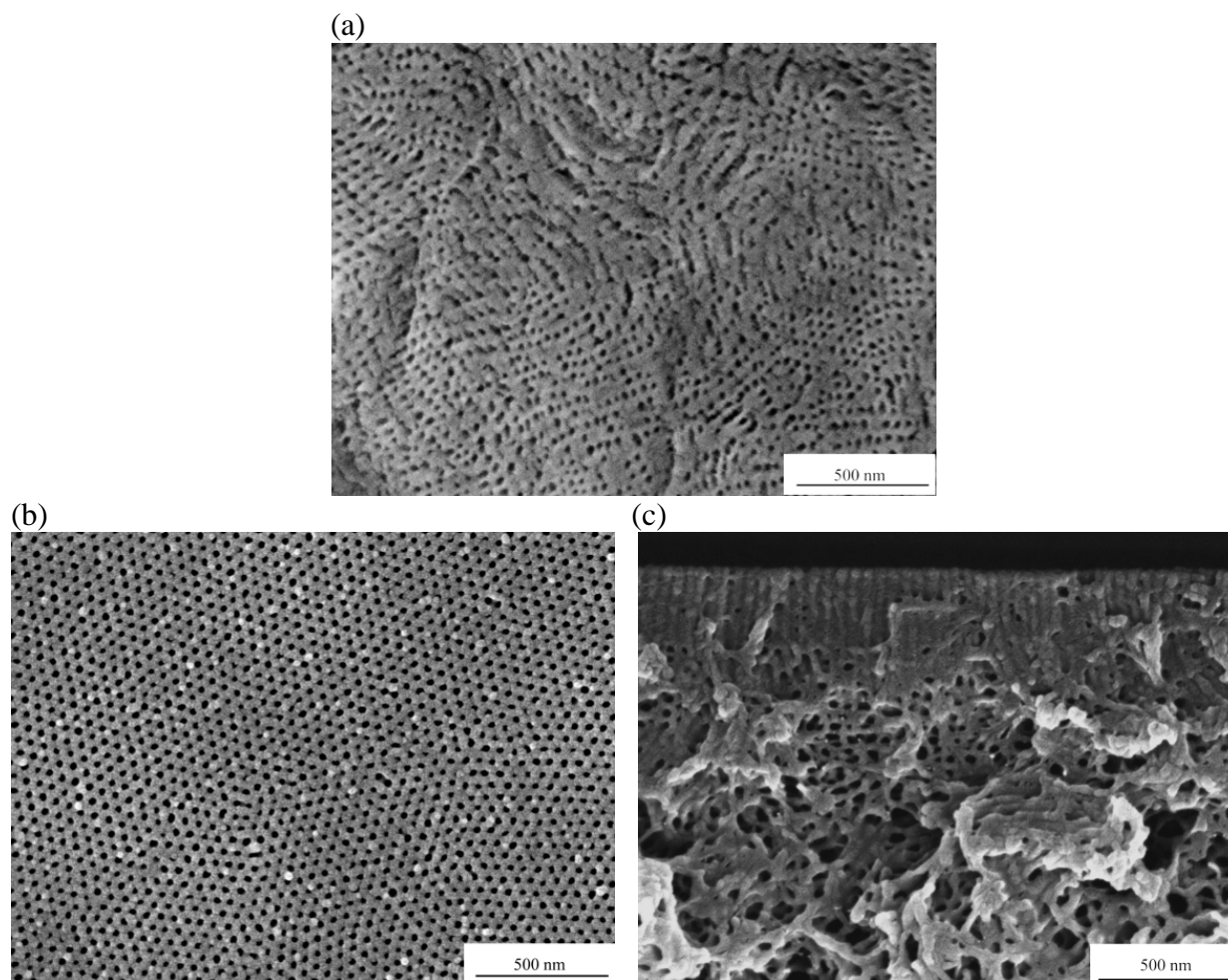


Figure 4: Cryo-SEM micrograph of (a) the casting solution of 26.5 wt% PS_{80.2}-*b*-P4VP_{19.8}¹⁴⁶ in THF/DMF: 35/65 and SEM micrographs of (b) the surface and (c) the cross section of the dried membrane. The evaporation time was 2 s.

As predicted by the solution investigations, a 2D hexagonally packed cylindrical structure has been formed in the final membrane surface layer (Figure 4 (b)) in the same way as in the solution. The cross section (Figure 4 (c)) consists of cylinders of an approximately 330 nm average height. The distance measured between the pores' centers was approximately 45 ± 3.0 nm, and the average pore size was found to be 20 ± 3.0 nm. Comparing the pore diameter and the pore distance found in the membrane with the results we got from the investigations of the solutions, shows that the distance between the pore centers agrees well with the domain spacing d found in SAXS and cryo-SEM results. The average pore diameter of the membrane relates well with the R_h of the P4VP homopolymer measured in the dilute solution, if we assume two touching but non-interpenetrating P4VP coils. The 4-fold of the R_h obtained by DLS (4.8 nm, see the relevant value in Table 3) leads to a domain diameter of 19.2 nm in solution which relates well with the average pore diameter of the final membrane (~20 nm). From this we can conclude that the P4VP chains are highly swollen and do not interdigitate significantly with other P4VP chains before the precipitation step. In the case of the PS matrix, the final diameter in solution results to approximately 28 nm, instead of 35 nm for non-interpenetrating coils. On the other hand, in the final membrane, the PS wall thickness is measured to be approximately 25 nm, instead of approximately 28 nm given from $R_h=7$ nm under θ -conditions (since $R_g = 10$ nm) for non-interpenetrating coils. The difference in both cases is probably caused by the tendency of the PS coils to interpenetrate with each other in solution or during membrane formation, as the selective solvent THF is partly evaporated leading to a significantly higher concentration of PS in the PS-rich domains, compared to a lower P4VP concentration in the P4VP rich domains. A longer evaporation time was also investigated for our system (5 sec), resulting in a selective membrane layer with larger pore diameters of 25 ± 4 nm (Figure 5).

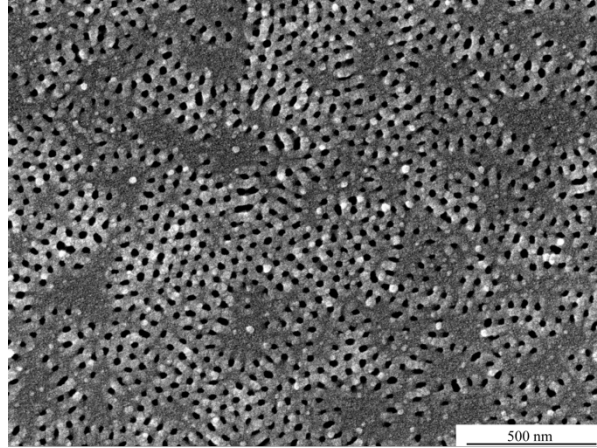


Figure 5: SEM micrograph of the membrane surface from the 26.5 wt% PS_{80.2}-*b*-P4VP_{19.8}¹⁴⁶ diblock copolymer solution in THF/DMF: 35/65. The evaporation time was 5 s.

As a lot of data on this type of diblock copolymer membranes is available, we checked the applicability of our results to other data reported before.[63] For this, we analyze the data of membranes resulting from casting solutions where the block copolymer was PS₈₁-*b*-P4VP₁₉¹⁶⁰ and the P4VP molecular weight in the diblock copolymer was 32k. The smallest pore size was found when the casting solution consists of 22 and 24 wt% block copolymer in solvent mixtures of THF/DMF: 60/40 and 50/50 while the evaporation time was 10 and 5 seconds, respectively. The average pore diameters for the specific mentioned evaporation times are calculated to be equal to 27 ± 5 nm and 29 ± 5 nm, while the theoretical R_h of the P4VP chain, proportional to the measured R_h by SLS in this work, is 5.1 nm leading to 4-fold of 20.4 nm P4VP diameter. For longer evaporation times (corresponding to higher polymer concentrations) the pore size increased which is a result of stronger segregation (as also seen in our SAXS data). Therefore, the relationship between the R_h of the pore forming block and the pore size of a membrane obtained by SNIPS holds only if the casting solution is very close to the disorder-order transition and the evaporation time for the cast block copolymer solution-cast film prior to phase inversion is kept short. An increase of evaporation time leads to larger pore sizes, however a too long evaporation time may destroy the aligned pore structure, as was discussed by Phillip et al. [45]

4 Conclusions

The aim of this work was to find correlations between the structural features of a block copolymer and its constituent blocks (as homopolymers) in solution on the one side and the final surface structure of the block copolymer membrane obtained by the SNIPS process on the other side. For this, we analyzed the size of the structural features of the diblock copolymer from dilute solution *via* concentrated solution and the final membrane. Also, we analyzed the size of corresponding homopolymers of the different blocks in dilute solution. In good solvent mixtures, at a very low concentration, a block copolymer composed of two incompatible blocks does not tend to form micelles but rather behaves like a free random coil. Micelles will be formed upon increase of the concentration in the solution. This work confirms the results of former studies that by casting a solution with a concentration close to the formation of an ordered structure, membranes with regular pore structures can be obtained. In addition, we showed that the resulting pore sizes relate in a simple way to the R_h of the pore forming block. At least in this system, the pore forming block seems to behave like a non-percolating coil filling the swollen pore before the phase inversion step.

However, for a generalization of this result chemically different block copolymers have to be analyzed in a similar way. Furthermore, other questions related to the structure formation of this type of membranes are still open. We still have to understand the detailed influence of solution viscosity and thermodynamic parameters of structural features such as the length of the cylindrical channels in the selective layer of the membrane and the detailed structure of the spongy or finger-like sublayer, as these have also a strong influence on the membrane performance.

Acknowledgments: The authors would like to thank Dr. Andreas Meyer (University of Hamburg) and Dr. Vasyl Haramus (Helmholtz-Zentrum Geesthacht) for very helpful scientific discussion (SAXS), Brigitte Lademann (Helmholtz-Zentrum Geesthacht) for polymer synthesis and Maren Brinkmann (Helmholtz-Zentrum Geesthacht) for polymer characterization. Part of this research was carried out at the light source PETRA III at DESY, a member of the Helmholtz Association (HGF).

References

1. Bates FS, Hillmyer MA, Lodge TP, Bates CM, Delaney KT, and Fredrickson GH. *Science* 2012;336(6080):434-440.
2. Mogi Y, Nomura M, Kotsuji H, Ohnishi K, Matsushita Y, and Noda I. *Macromolecules* 1994;27(23):6755-6760.
3. Bronstein L, Seregina M, Valetsky P, Breiner U, Abetz V, and Stadler R. *Polymer Bulletin* 1997;39(3):361-368.
4. Schmalz H, Müller AJ, and Abetz V. *Macromolecular Chemistry and Physics* 2003;204(1):111-124.
5. Hückstädt H, Göpfert A, and Abetz V. *Polymer* 2000;41(26):9089-9094.
6. Georgopoulos P, Handge UA, Abetz C, and Abetz V. *Polymer* 2016;104:279-295.
7. Hiekkataipale P, Löbbling TI, Poutanen M, Priimagi A, Abetz V, Ikkala O, and Gröschel AH. *Polymer* 2016;107:456-465.
8. Hadjichristidis N, Tselikas Y, Iatrou H, Efstratiadis V, and Avgeropoulos A. *Journal of Macromolecular Science, Part A: Pure and Applied Chemistry* 1996;33(10):1447-1457.
9. Tselikas Y, Iatrou H, Hadjichristidis N, Liang K, Mohanty K, and Lohse D. *The Journal of Chemical Physics* 1996;105(6):2456-2462.
10. Hückstädt H, Göpfert A, and Abetz V. *Macromolecular Chemistry and Physics* 2000;201(3):296-307.
11. Matsushita Y, Hayashida K, and Takano A. *Macromolecular Rapid Communications* 2010;31(18):1579-1587.
12. Ruotsalainen T, Turku J, Hiekkataipale P, Vainio U, Serimaa R, ten Brinke G, Harlin A, Ruokolainen J, and Ikkala O. *Soft Matter* 2007;3(8):978-985.
13. Faber M, Hofman AH, Polushkin E, van Ekenstein GA, Seitsonen J, Ruokolainen J, Loos K, and ten Brinke G. *Macromolecules* 2013;46(2):500-517.
14. Hofman AH, Reza M, Ruokolainen J, ten Brinke G, and Loos K. *Macromolecules* 2014;47(17):5913-5925.
15. Hofman AH, Reza M, Ruokolainen J, ten Brinke G, and Loos K. *Angewandte Chemie International Edition* 2016;55(42):13081-13085.
16. Abetz V and Boschetti-de-Fierro A. 7.02 - Block copolymers in the condensed state. *Polymer science: a comprehensive reference*, vol. 7. Amsterdam: Elsevier, 2012. pp. 3-44.
17. Bates F and Fredrickson G. *Physics Today* 1999;52(2):32-38.
18. Alexandridis P and Lindman B. *Amphiphilic block copolymers: self-assembly and applications*. Amsterdam: Elsevier, 2000.
19. Krause S. *The Journal of Physical Chemistry* 1964;68(7):1948-1955.
20. Utiyama H, Takenaka K, Mizumori M, Fukuda M, Tsunashima Y, and Kurata M. *Macromolecules* 1974;7(4):515-520.
21. Tuzar Z and Kratochvil P. *Advances in Colloid and Interface Science* 1976;6(3):201-232.
22. Antonietti M, Heinz S, Schmidt M, and Rosenauer C. *Macromolecules* 1994;27(12):3276-3281.
23. Zhang L and Eisenberg A. *Science* 1995;268(5218):1728.
24. Zhang L, Yu K, and Eisenberg A. *Science* 1996;272(5269):1777.
25. Zhang L, Bartels C, Yu Y, Shen H, and Eisenberg A. *Physical Review Letters* 1997;79(25):5034.
26. Clarke C, Eisenberg A, La Scala J, Rafailovich M, Sokolov J, Li Z, Qu S, Nguyen D, Schwarz S, and Strzhemechny Y. *Macromolecules* 1997;30(14):4184-4188.
27. Hamley IW. *Block copolymers in solution: fundamentals and applications*. New York: John Wiley & Sons, 2005.
28. Lazzari M, Liu G, and Lecommandoux S. *Block copolymers in nanoscience*. Weinheim: Wiley-VCH, 2007.

29. Mai Y and Eisenberg A. *Chemical Society Reviews* 2012;41(18):5969-5985.
30. Oss-Ronen L, Schmidt J, Abetz V, Radulescu A, Cohen Y, and Talmon Y. *Macromolecules* 2012;45(24):9631-9642.
31. Marques DS, Dorin RM, Wiesner U, Smilgies D-M, Behzad AR, Vainio U, Peinemann K-V, and Nunes SP. *Polymer* 2014;55(6):1327-1332.
32. Stegelmeier C, Exner A, Hauschild S, Filiz V, Perlich J, Roth SV, Abetz V, and Förster S. *Macromolecules* 2015;48(5):1524-1530.
33. Gröschel AH, Walther A, Löbbling TI, Schacher FH, Schmalz H, and Müller AH. *Nature* 2013;503(7475):247-251.
34. Ruckdäschel H, Sandler JK, Altstädt V, Rettig C, Schmalz H, Abetz V, and Müller AH. *Polymer* 2006;47(8):2772-2790.
35. Bahrami R, Löbbling TI, Schmalz H, Müller AH, and Altstädt V. *Polymer* 2017;109:229-237.
36. Kirschnick T, Gottschalk A, Ott H, Abetz V, Puskas J, and Altstädt V. *Polymer* 2004;45(16):5653-5660.
37. Abetz V and Goldacker T. *Macromolecular Rapid Communications* 2000;21(1):16-34.
38. Chao C-C, Wang T-C, Ho R-M, Georgopoulos P, Avgeropoulos A, and Thomas EL. *ACS Nano* 2010;4(4):2088-2094.
39. Metz SJ, Mulder MHV, and Wessling M. *Macromolecules* 2004;37(12):4590-4597.
40. Rahman MM, Filiz V, Shishatskiy S, Abetz C, Georgopoulos P, Khan MM, Neumann S, and Abetz V. *ACS Applied Materials & Interfaces* 2014;7(23):12289-12298.
41. Yang SY, Ryu I, Kim HY, Kim JK, Jang SK, and Russell TP. *Advanced materials* 2006;18(6):709-712.
42. Peinemann KV, Abetz V, and Simon PFW. *Nature Materials* 2007;6(12):992-996.
43. Schacher F, Rudolph T, Wieberger F, Ulbricht M, and Müller AH. *ACS Applied Materials & Interfaces* 2009;1(7):1492-1503.
44. Jackson EA and Hillmyer MA. *ACS Nano* 2010;4(7):3548-3553.
45. Phillip WA, Hillmyer MA, and Cussler E. *Macromolecules* 2010;43(18):7763-7770.
46. Qiu X, Yu H, Karunakaran M, Pradeep N, Nunes SP, and Peinemann K-V. *ACS Nano* 2013;7(1):768-776.
47. Mulvanna RA, Weidman JL, Jing B, Pople JA, Zhu Y, Boudouris BW, and Phillip WA. *Journal of Membrane Science* 2014;470:246-256.
48. Hahn J, Clodt J, Filiz V, and Abetz V. *RSC Advances* 2014;4(20):10252-10260.
49. Clodt JI, Bajer B, Buhr K, Hahn J, Filiz V, and Abetz V. *Journal of Membrane Science* 2015;495:334-340.
50. Abetz V. *Macromolecular Rapid Communications* 2015;36(1):10-22.
51. Radjabian M, Koll J, Buhr K, Handge UA, and Abetz V. *Polymer* 2013;54(7):1803-1812.
52. Radjabian M, Koll J, Buhr K, Vainio U, Abetz C, Handge UA, and Abetz V. *Polymer* 2014;55(13):2986-2997.
53. Noor N, Koll J, Radjabian M, Abetz C, and Abetz V. *Macromolecular Rapid Communications* 2015.
54. Sankhala K, Koll J, Radjabian M, and Abetz V. *Advanced Materials Interfaces* 2017, DOI: 10.1002/admi.201600991.
55. Hahn J, Clodt JI, Abetz C, Filiz V, and Abetz V. *ACS Applied Materials & Interfaces* 2015;7(38):21130-21137.
56. Stegelmeier C, Filiz V, Abetz V, Perlich J, Fery A, Ruckdeschel P, Rosenfeldt S, and Förster S. *Macromolecules* 2014;47(16):5566-5577.
57. Eggers S, Lauterbach F, and Abetz V. *Polymer* 2016;107:357-367.
58. Clodt JI, Rangou S, Schroder A, Buhr K, Hahn J, Jung A, Filiz V, and Abetz V. *Macromolecular Rapid Communications* 2013;34(2):190-194.

59. Gallei M, Rangou S, Filiz V, Buhr K, Bolmer S, Abetz C, and Abetz V. *Macromolecular Chemistry and Physics* 2013;214(9):1037-1046.
60. Yu H, Qiu X, Nunes SP, and Peinemann K-V. *Angewandte Chemie International Edition* 2014;53(38):10072-10076.
61. Dorin RM, Marques DS, Sai H, Vainio U, Phillip WA, Peinemann K-V, Nunes SP, and Wiesner U. *ACS Macro Letters* 2012;1(5):614-617.
62. Radjabian M, Abetz C, Fischer B, Meyer A, and Abetz V. *ACS Applied Materials & Interfaces* 2017, DOI: 10.1021/acsami.6b15199.
63. Rangou S, Buhr K, Filiz V, Clodt JI, Lademann B, Hahn J, Jung A, and Abetz V. *Journal of Membrane Science* 2014;451:266-275.
64. Hansen CM. *Hansen solubility parameters: a user's handbook*: CRC press, 2007.
65. Barton AF. *Handbook of polymer-liquid interaction parameters and solubility parameters*: CRC Press, 1990.
66. James M, Goncalves-Miskiewicz M, May PE, Nanson L, Effenberger R, Bonrad K, Pan J, and Kluge E. Patent: Compositions comprising polymeric binders. 2011.
67. Alberda van Ekenstein G, Meyboom R, Ten Brinke G, and Ikkala O. *Macromolecules* 2000;33(10):3752-3756.
68. Bates FS and Fredrickson GH. *Annual Review of Physical Chemistry* 1990;41(1):525-557.
69. Schärfl W. *Light scattering from polymer solutions and nanoparticle dispersions*. Berlin Heidelberg: Springer-Verlag Berlin Heidelberg, 2007.
70. Kratochvíl P. *Classical light scattering from polymer solutions*. Amsterdam: Elsevier, 1987.
71. Teraoka I. *Frontmatter and Index. Polymer Solutions: An Introduction to Physical Properties*. New York, USA: John Wiley & Sons, Inc., 2002.
72. Sperling LH. *Introduction to physical polymer science*. New York: John Wiley & Sons, 2005.
73. Brandrup J, Immergut EH, Grulke EA, Abe A, and Bloch DR. *Polymer Handbook*. New York: John Wiley & Sons, 1989.
74. Brown W and Mortensen K. *Scattering in polymeric and colloidal systems*: CRC Press, 2000.
75. Ogawa H, Takenaka M, Miyazaki T, Fujiwara A, Lee B, Shimokita K, Nishibori E, and Takata M. *Macromolecules* 2016;49(9):3471-3477.

Highlights

- Investigation of structure formation from dilute solution to concentrated solution and to the final membrane
- Membrane formation with regular pore size *via* SNIPS by casting a solution very close to structure formation
- Final membrane pore size relate to the hydrodynamic radius of the pore forming block